Computer Methods in Biomechanics and Biomedical Engineering

Publication details, including instructions for authors and subscription information:
http://www.tandfonline.com/loi/gcmb20

Automated localisation and boundary identification of superficial femoral artery on MRI sequences

Tzung-Chi Huang [a], Da-Chuan Cheng [a], Arno Schmidt-Trucksäss [b] & Uwe H. Schütz [c]

[a] Department of Biomedical Imaging and Radiological Science, China Medical University, Taichung, Taiwan

[b] Institute of Exercise and Health Sciences, Sports Medicine, Vascular Lab, University Basel, Basel, Switzerland

[c] Department of Diagnostic and Interventional Radiology, University Hospital of Ulm, Ulm, Germany

Available online: 06 Jan 2012

To cite this article: Tzung-Chi Huang, Da-Chuan Cheng, Arno Schmidt-Trucksäss & Uwe H. Schütz (2012): Automated localisation and boundary identification of superficial femoral artery on MRI sequences, Computer Methods in Biomechanics and Biomedical Engineering, DOI:10.1080/10255842.2011.643468

To link to this article: http://dx.doi.org/10.1080/10255842.2011.643468

Computer Methods in Biomechanics and Biomedical Engineering
iFirst article, 2011, 1–12

Automated localisation and boundary identification of superficial femoral artery on MRI sequences

Tzung-Chi Huang[a], Da-Chuan Cheng[a]*, Arno Schmidt-Trucksäss[b] and Uwe H. Schütz[c]

[a]*Department of Biomedical Imaging and Radiological Science, China Medical University, Taichung, Taiwan;* [b]*Institute of Exercise and Health Sciences, Sports Medicine, Vascular Lab, University Basel, Basel, Switzerland;* [c]*Department of Diagnostic and Interventional Radiology, University Hospital of Ulm, Ulm, Germany*

(*Received 7 June 2011; final version received 20 November 2011*)

In this paper, an automated method to localise the right superficial femoral artery (SFA) and identify its boundary on magnetic resonance imaging (MRI) sequences without contrast medium injection is proposed. Some anatomical knowledge combined with the mathematical morphology is used to distinguish SFA from other vessels. Afterwards, the directional gradient, continuity and the local contrast are applied as features to identify the artery's boundary using dynamic programming. The accuracy analysis shows that the system has average unsigned errors 3.1 ± 3.1% on five sequences compared to experts' manual tracings.

Keywords: superficial femoral artery; boundary detection; dynamic programming

1. Introduction

Arterial flow to the working musculature is the dominant stimulus for arterial diameter through shear stress (Langille and O'Donnell 1986). Cross-sectional studies consistently show higher femoral diameter in endurance-trained subjects than in untrained subjects (Schmidt-Trucksäss et al. 2000; Huonker et al. 2003). After training untrained men, femoral artery diameter increased significantly compared to the control subjects (Dinenno et al. 2001; Thijssen et al. 2007). In the Trans Europe Foot Race (TEFR) study, the effect of a multistage ultramarathon over 4487.7 km in 64 days without 1 day rest on the structure and function of different organ systems will be analysed. Whether an increase in diameter is possible in already endurance-trained subjects due to an extraordinary stimulus has not been shown before. For this purpose, a sub-study of TEFR09 dealing with the arterial system was presented in this study.

The aim of the present study is to develop and validate a novel automatic superficial femoral arterial wall detection algorithm in magnetic resonance imaging (MRI) sequences over several heart cycles. Data will be compared to manual tracings in order to precisely determine femoral diastolic and systolic diameter changes along time and the superficial femoral artery (SFA) local compliance. Evaluation of local compliance of the arterial wall of SFA is possible, when the maximal systolic and diastolic vessel diameter is combined with additional simultaneous blood pressure data. In particular, we want to know whether highly endurance-trained individuals adapt the diameter of the femoral artery due to chronic increase in shear stress by the ultra-endurance race. In order to see the changes over time, measurements with a high accuracy and reproducibility are necessary and the SFA will be examined with native vascular MRI. Due to the natural limited compliance of the subjects (endurance athletes), contrast media were not usable for vascular MRI in this study.

Previous studies regarding the vessel boundary detection include the processing of longitudinal view (Liang et al. 2000; Tang and Acton 2004; Cheng and Jiang 2008; Cheng et al. 2010) and cross-sectional view (Zhu et al. 2002; Kim and Park 2004; Doulaverakis et al. 2010; Cheng et al. 2011). Without contrast medium, the magnetic resonance angiography (MRA) and sonography are often used to observe and quantify the artery's characteristics. MRI is a powerful means of non-invasively imaging the blood vessels in the human body. It can be used not only to visualise the vessel but also to quantify the cross-sectional area. However, errors of the cross-sectional area may result from intraluminal saturation effects, poor resolution and signal-to-noise ratio. In practice, the physician can tolerate relative errors less than 5%. The dependence of vessel area accuracy and precision as a function of MRI parameters was shown previously (Jiang et al. 2007). In addition, the study regarding the superficial artery's boundary detection in MRA without contrast medium injection is reported (Law and Chung 2007). Another previous study uses the grey-level contrast for the information in boundary detection on intravascular

*Corresponding author. Email: dccheng@mail.cmu.edu.tw

ISSN 1025-5842 print/ISSN 1476-8259 online

http://dx.doi.org/10.1080/10255842.2011.643468
http://www.tandfonline.com

ultrasound images (Zhu et al. 2002). The present study will also use the grey-level local contrast. However, we use it as additional information to predict the cross-sectional area before the boundary detection. The mathematical model using the local contrast as information to predict the cross-sectional area is described in the Appendix.

The significance of this study includes the following: (1) we propose a fully automated algorithm to detect and localise the centre of the SFA in MRI; (2) we propose a fully automated algorithm to identify the boundary of the SFA; and (3) we develop a mathematical model to prove the correlation between the local contrast curve and the area curve. Therefore, the diameter of artery can be predicted *via* samplings. The second algorithm is not specific; it can be used to identify other artery's boundary in MRA sequences without the contrast medium injection, with the known centre position and its rough radius to define a region of interest.

The rest of this paper is organised as follows. The image sources and the MRI protocol are introduced in Section 2.1. Section 2.2 describes how the manual tracings are performed. In Section 2.3, we propose a method to detect the centre position of SFA lumen. In Section 2.4, the circle model and the grey-level local contrast is used to guide the dynamic programming for the SFA's boundary identification. Afterwards, the results are given in Section 3. We then discuss the properties of the proposed scheme in Section 4. Finally, the conclusion is given in Section 5.

2. Materials and methods

2.1 Image acquisition

As recently described, a mobile MRI (Siemens – type 'Avanto™', 1.5 T, Siemens Ltd, Erlangen, Germany) was used for image acquisition (Cheng et al. 2011). Twelve out of 44 participants in the TEFR09 study (DFG Project GZ: SCHU 2514/1-1, AOBJ: 565344) took part in this study after approval of the local ethics committee of Ulm University in accordance with the Declaration of Helsinki. Complete MRI sequences were obtained in all subjects. To validate the novel detection algorithm of the SFA lumen presented in this study, several MRI sequences of the selected subjects were randomly chosen.

A mobile 1.5 T Magnetom (Siemens – Avanto™, Model Mob. MRI 02.05, Siemens Ltd) having a flexible six-channel body matrix coil with six integrated low-noise preamplifiers (Siemens Ltd) and bilateral table fixation were used for acquisition of MRI sequences of the SFA from subjects. The athletes were fixed in a stretched supine position and head forward on the MR table.

To identify the axial perpendicular acquisition location at the right SFA 10 mm beneath the bifurcation of the common femoral artery, a biplanar coronal and sagittal localiser ('true fast imaging with steady state precision'; Siemens Ltd) was used. In analogy to the common carotid artery MR measurement (Cheng et al. 2011), change of the SFA diameter during systole and diastole was assessed with a T2*-weighted gradient-spoiled, gradient-echo, cine sequence ('fast low angle shot', Siemens Ltd) in a 2D cross-sectional view with the prospective 2D electrocardiogram (ECG) gating (cardiac triggering). Specific sequence parameters were set to be the following: flip angle 15°, echo time variable between 4 and 6 ms (depending on heart rate), repetition time variable between 20 and 40 ms (depending on heart rate), slice thickness 6 mm, field of view 768 cm^2, matrix size 512 × 384, pixel size 0.625 mm ISO, pixel bandwidth 250 and number of images per sequence: 50 images for one RR cycle (approximately 300 heart beats per sequence). Total imaging acquisition time was approximately 4 min 30 s to 5 min for each sequence (Table 1).

2.2 Manual tracings

Two well-trained readers familiar with MRIs of the pelvic region performed the manual tracings of the SFA in a random order. Five sequences from five different subjects were traced manually and independently. Each two manual tracings made by different readers on the same sequence were averaged to form a standard. Finally, the automated results were compared to the manual tracings and the accuracy was calculated. The manual tracings were performed on a graphic user interface (GUI) software designed by ourselves. It can resize the image and allow the reader to operate it in a sub-pixel scale (Figure 6).

2.3 SFA localisation

The SFA can be seen on MRI if the blood flow speed is relatively large. In our previous study (Cheng et al. 2011), however, the flow speed variation in the SFA is larger than that in the common carotid artery. Therefore, the method described in Cheng et al. (2011) cannot be used in this study. In Cheng et al. (2011), the carotid artery can be seen

Table 1. The average unsigned relative error on five sequences.

	Sequence 1 (%)	Sequence 2 (%)	Sequence 3 (%)	Sequence 4 (%)	Sequence 5 (%)	Average (%)
Mean	2.61	2.36	3.65	4.57	2.42	3.12
SD	2.82	2.94	3.86	4.00	1.99	3.12

Note: Each sequence contains 50 images.

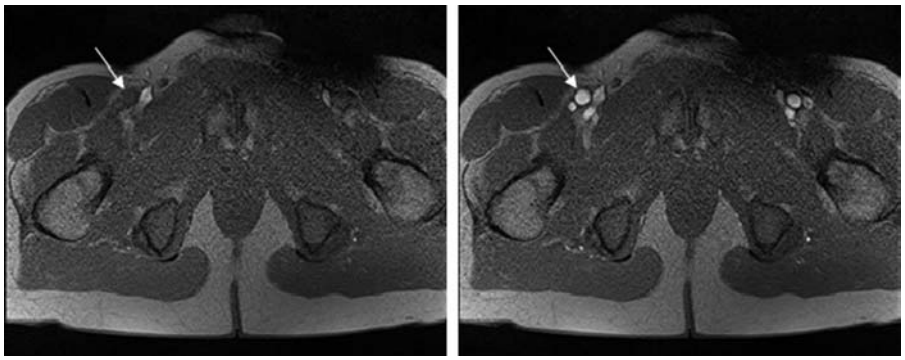

Figure 1. SFA on MRA raw images for (a) slow blood flow speed and (b) fast blood flow speed for the same patient in different flood flow phase.

on every image in the sequence, and therefore it can be identified using a single image. However, it is very different in the SFA's image. Figure 1 shows two succeeding images in an image sequence. The arteries cannot be seen in (a) but can be seen in (b). Moreover, there are two or three vessels near around which result in difficulties to recognise the SFA. They have the same blood flow phase to the SFA. The difficulties of SFA localisation are stated as follows:

(1) The SFA cannot be seen on every image. The grey values of the SFA vary according to its blood flow velocity. In some images, the artery boundaries are vague and almost impossible to be detected.
(2) Some vessels are close to the SFA.
(3) The size of the SFA is normally large but not the largest one and it is also patient dependent.

We will explore the above-described issues and propose our strategies as follows:

(1) The arteries can be seen only when their blood flow velocity is fast. The intravascular signal intensity is an increasing function of the blood flow, but there is no constant proportional dependency. If the blood flow speed is slow, then the grey value is small and the artery lumen appears dark. Therefore, the artery's boundary is vague. For example, the grey values of the SFA in the sequence (Figure 1) range from 57 to 170, and the background near the artery ranges from 60 to 100. Since the SFA is not seen on every image, it is impossible to localise the artery position in each static image. Fortunately, the SFA position does not change during the sequence. The patient movement and artefact caused by breathing are very limited. Therefore, we can use the whole sequence information to localise the artery's position.
(2) Some arteries and veins are very close to the SFA. Especially the blood flow phases of arteries are also very similar so that the images are similar. They become light and dark together. During the low blood flow phase, the boundaries of all arteries are almost invisible. In Figure 1(b), we can see that the wall of the SFA and the branches of the common femoral vein are attached together, but can still be distinguished by their shapes. The shape of artery is near round and the shape of vein might be very different.
(3) The cross-sectional area of the SFA is relatively large compared to the other arteries nearby. It is normally the largest artery; however, there are exceptions. Their size can be one of the special features but not the unique factor. The relative position may be another factor.

Based on the analysis of the above three issues, we develop a strategy to localise the SFA. Due to the fact that the artery blood flow velocity is not consistent, it appears sometimes light and sometimes dark. On the contrary, the blood flow velocity in veins does not change significantly. The variance or standard deviation of grey value changes in time, and can be an effective feature to distinguish arteries from other tissues such as veins and muscles. To do this, all 50 images are loaded and put them in a 3D matrix. Thereafter, the standard deviation of grey value along different images of each pixel on image is calculated [Figure 2(a)]. These values reveal variance in the blood flow velocity. Larger variance represents larger flow velocity variance. It can be observed that the arteries have larger intensities, and hence the variance image becomes easier to be segmented from other tissues than the original images. Let $I_n(x, y)$ be the grey value at (x, y) on raw image number n. The variance image can be calculated by

$$V(x,y) = \sqrt{\frac{1}{N-1}\sum_{n=1}^{N}\left(I_n(x,y) - \bar{I}(x,y)\right)^2}.$$

So far we have resolved the first issue. The next task is to distinguish the SFA among all vessels. In order to speed up

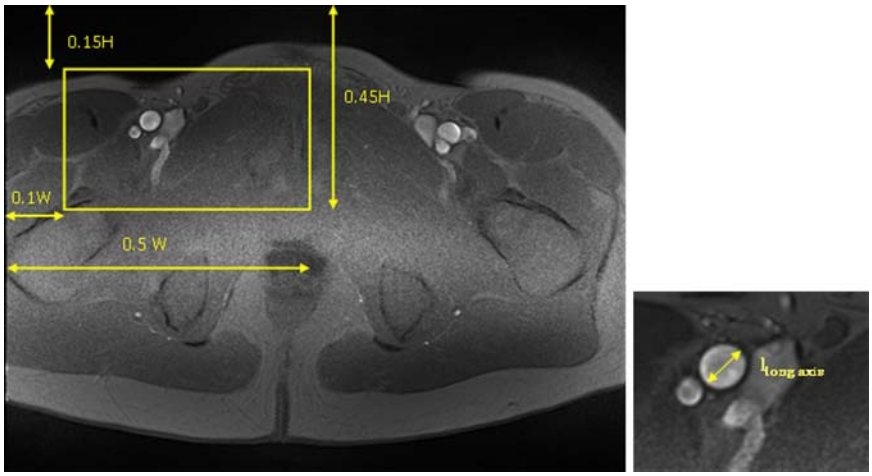

Figure 2. (a) The variance image and the ROI (R_V: denoted by the rectangle). (b) After the PCA process, the long axis and short axis is computed and their length ratio is used to be one of the features.

the computation time and to reduce the noise effect, an region of interest (ROI) is set. Since we are interested in the right SFA (left-hand side on the image), only possible area is selected. The upper and the lower bound of the ROI are set to be 15% and 45% of the image height. The left and the right bound are set to be 10% and 50% of the image width [Figure 2(a)]. The rectangle in Figure 2(a) is an example of the ROI. The SFA is included in this ROI. Let R_V denote the sub-image (ROI) extracted from the variance image V. The following process is applied only on R_V.

The top-hat technique (Dougherty 1992) is applied to remove the uneven background. Top-hat transform is an operation that extracts small elements and details from the given images in mathematical morphology. It is defined as follows:

$$R_1 = T(f) = f - (f \circ s), \tag{1}$$

where $f = R_V$ is the image to be transformed, s is the structural element (with a radius 15 pixels and a disc shape in this study) and '$\circ$' is the opening operation in mathematical morphology. The uneven background is resulted from the nonhomogeneous magnetic field. They are usually distributed in the middle part of the body where full of interstitial fluid. After the top-hat transform, the ROI is homogeneous and thus Otsu's threshold technique (Otsu 1979) is applied to get a threshold value (T). This threshold is used to transform R_1 into a binary image R_2 as follows:

$$R_2(x,y) = \begin{cases} 1 & \text{if } R_1(x,y) > T \\ 0 & \text{otherwise} \end{cases} \quad \text{for all } (x,y) \text{ in } R_1 \tag{2}$$

The rest of the binary image R_2 contains many vessels, and the SFA is among them. To extract the SFA in the first step, the binary opening operation is applied to remove the salt-and-pepper noises. This opening operation can cut off some possible connected parts into separated parts, such as two vessels that are located closely. The structural element (s_2) used here is having a radius of 2 pixels with a disc shape (a 5×5 matrix). The opening operation is defined to be $R_3 = (R_2 \circ s_2)$. The second step is to label each connected region, count area of each label and find the central locations (coordinates) of all labelled vessels. This step is applied on R_3.

Here, we use three features to discriminate SFA from all vessels: axes ratio, area ratio and distance. They are defined as follows. The ratio of ith axes is defined as

$$r_{\text{axis}}(i) = \frac{l_{\text{long axis}}(i)}{l_{\text{short axis}}(i)} - 1, \tag{3}$$

where $l_{\text{long axis}}$ is the length of the long axis and $l_{\text{short axis}}$ is the length of the short axis after principal component analysis (PCA) (Jolliffe 1986; Gorban and Zinoyyev 2009) on each artery's cross-sectional area [Figure 2(b)]. The feature $r_{\text{axis}} > 0$ indicates the shape of the vessel. A smaller value denotes that the vessel has a circular boundary, which is usually an artery. A larger value represents that the cross-sectional view is oval or elliptic, which is usually a vein.

Before the area ratio is computed, areas less than 40 pixels are removed. The diameter of SFA is about 6.7 ± 0.3 (range 5.9–8.2) mm (Radegran and Saltin 2000). The pixel size is 0.625 mm in our MRA images. Therefore, the radius of SFA in our images should be larger than 4 pixels, which represents an area size of 50 pixels. For safety we reduce the threshold from 50 ($= 4^2\pi$) to 40 pixels. This is to remove the rest noise and some small vessels so that the SFA can be easily identified. The area ratio is defined as follows:

$$r_{\text{area}}(i) = \frac{A_{\min}}{A_i}, \tag{4}$$

where $A_{\min}$ is the smallest area among all vessels and $r_{\text{area}}(i)$ denotes the ith area ratio, $0 < r_{\text{area}} \leq 1$. Since the SFA is one of the largest arteries, smaller value denotes a larger possibility and larger values represent smaller vessels.

We shall now discuss the distance feature. It is a normalised distance between each vessel centre and the centre of all the vessels' centres. It is defined as follows:

$$d_i' = \|\vec{v}_i - \bar{v}\|, \quad d_i = \frac{d_i'}{\max_i d_i'}, \tag{5}$$

where $\vec{v}_i$ denotes the ith artery centre, $\bar{v}$ is the mean of all $\vec{v}_i$, $\|\cdot\|$ is the Euclidean distance and $0 < d_i \leq 1$ is the normalised distance feature. The reason for using the distance feature is that, we have observed in most cases, the SFA is located in the middle-upside of all detected vessels. The smaller value of d_i is expected to represent the SFA. Through the above features, we are able to detect the position of the SFA with the following cost function:

$$c^* = \min_i r_{\text{axis}}(i) r_{\text{area}}(i) + \alpha d_i, \tag{6}$$

where α is a weighting factor and c is the cost value. The optimal solution (i^*) is the one having the minimum value in Equation (6). After the SFA's centre is determined, its radius can be measured simply by:

$$\text{raidus} = \text{int}\frac{l_{\text{long axis}}(i^*)}{2},$$

where $l_{\text{long axis}}$ denotes its major axis length in the detected region in R_3. The 'int(·)' function denotes the round-off mode. This radius is only for an ROI chosen in the following dynamic programming procedure.

Summary of the algorithm:

Step 1: Input all images of an image sequence. Build the variance image.
Step 2: Cut off the ROI to be R_V (Figure 2).
Step 3: Apply top-hat filter on R_V to remove the uneven background and output R_1 [Equation (1)].
Step 4: Transform R_1 to a binary image R_2 using Otsu's thresholding technique [Equation (2)].
Step 5: Apply opening operation on R_2 and output R_3.
Step 6: Remove spots whose area is less than 40 pixels (Figure 3).
Step 7: Label the rest spots; calculate the three features for all spots: r_{axis}, r_{area}, and d_i [Equation (3)–(5)].
Step 8: Output the centre (c_x, c_y) and the radius of the spot having the minimal cost value in Equation (6).

2.4 SFA boundary identification

The round shaped feature of artery is important. It is used to avoid possible errors caused by local noises. These errors include the heterogeneous gradient obtained in the artery lumen and at the boundary. To alleviate this problem, we have proposed a circle model to guide the dynamic programming (Cheng et al. 2011). However, the method in Cheng et al. (2011) cannot be applied directly. This is because the method in Cheng et al. (2011) is to detect the carotid artery wall. The blood flow speed in the carotid artery is faster than the flow speed in the SFA. In some MRA images containing the SFA, the SFA wall is very hard to be recognised compared with the images containing the carotid artery. We have modified it and added more information in the cost function. Dynamic programming is a method of solving complex problems by breaking them down into simpler steps commonly used in mathematics and computer science (Dasgupta et al. 2008). It is applicable in image processing to solve optimal problems such as finding a minimum (or maximum) with some given constraints (Cheng and Jiang 2008; Cheng et al. 2010). However, the limitation of this technique in images is that it cannot solve the closed form contour. One solution is to transform the image from Cartesian coordinate to polar coordinate (Domínguez and Nandi 2007) and then apply the dynamic

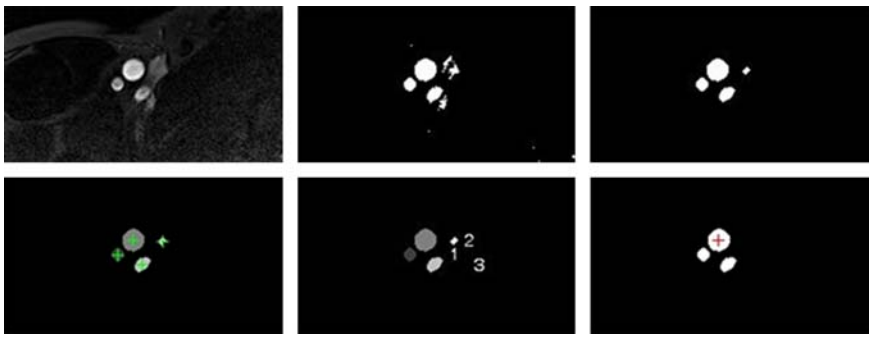

Figure 3. Results of Section 2.3. (a) The sub-image (R_1) after the top-hat transform from the variance image. (b) The binary image (R_2) after Otsu's thresholding technique. (c) The results (R_3) after the morphologic opening operation. (d,e) All arteries are labelled and their centres are calculated. (f) After the features are calculated, the SFA can be identified and its centre position and radius are calculated.

programming on the polar coordinate. Note that this procedure applies only on an ROI. However, two preconditions have to be satisfied: (1) the rough centre position of the object to be detected is known; (2) the sampling lines radiated from the object centre can at most sample one boundary point. Our problem meets these two preconditions.

The dynamic programming is issued in details as follows. We define the ROI extracted from R_3 to be R_s. The centre of R_s is the SFA centre detected in Section 2.3. Let M denote the number of rows and columns of R_s, where $M = \text{int}(1.5 \cdot \text{radius})$. In Cheng et al. (2011), we have developed the directional gradient. Apply directional gradient on R_s and output another matrix R_e Normalisation is applied on R_e, so that values range from -1 to 1, i.e. $-1 \leq R_e \leq 1$. Since the centre of R_e is the artery centre, we transform R_e to the polar representation and denote it as R_p, $R_p \in R^{(2M+1) \times \text{int}(2\pi M)}$. The x-axis of R_p represents angle ($0 \leq \theta \leq 2\pi$) and the y-axis represents the distance to the centre point in R_e. Notably, $\theta = 2\pi$ represents the start point copied to the end of the matrix R_p to convince the continuity between the start and end point. The dynamic programming is then searching a curve from left to right in R_p, which represents the artery boundary. Some features are taken into consideration in the design of the cost function. For convenience, we redefine the size of matrix R_p to be $M \times N$.

(1) Curve continuity: A variable for continuity is considered. Let d_r denote the maximal range that nodes in column $x - 1$ are allowed to jump onto the next column x in either up or down directions. Therefore, each node has maximum $(2d_r + 1)$ possible link paths to its previous column. If d_r is set larger, both the curve's roughness and the computation time are increased. The smoothness of the curve is quantified by the cost function.

(2) Circle model: The circle model having a known radius is embedded into the structure to guide the dynamic programming. This is based on the fact that the artery boundary is near round and the radius is estimated by the method described in Section 2.3. A Gaussian model is used to generate the strength how strong the dynamic programming is guided by the circle model. Let r denote the known circle radius, the strength is formulated as

$$-\frac{1}{\sigma}\exp\left(-\frac{(y-r)^2}{2\sigma^2}\right),$$

where σ is a variable controlling the strength of the guide. For small σ, the Gaussian has a thin but a sharp shape and the circle model has a larger effect on the result, i.e. it is more a circle-like boundary. For large σ, the Gaussian term vanishes and it works like a normal dynamic programming without the circle model. Since y and r are both integers, a look-up table can be set to reduce the computation time.

(3) Directional gradient: The directional gradients are the basic information to detect the artery boundary accurately. Negative gradients denote the artery boundary, while the positive gradients denote other boundary and are treated as noises.

(4) Local contrast: The first issue described in Section 2.3 is that the SFA has less contrast to its surrounding neighbourhood. In the worst case, even a medical expert cannot tell the exact boundary location. To solve this problem, we have to use the sequential image information and the local contrast. The sequential image information works like a memory to remember the boundary that has large local contrast. We observed that the local contrast curve and the area curve are correlated. Therefore, they can be used as a feature to guide the boundary identification. The local contrast is defined by calculating the grey-level variance in the sub-image R_s. Thus, each image has a local contrast value. The local contrast is normalised to be in the range [0.01–1]. The value of σ used in the circle model is determined by $\sigma = 2 + \text{contrast}(i)$, where 'contrast' denotes the local contrast and 'i' denotes the ith image.

Thus, the boundary detection problem is then transformed to an optimisation problem, which searches an optimal contour:

$$p_1^* p_2^* p_3^* \ldots p_N^* = \arg\min\left\{\sum_{i=1}^{N} R_p(p_i) | p_1 p_2 p_3 \ldots p_n\right\} \quad (7)$$

subject to some constraints,

where p_i is the point on the ith column in the matrix R_p, and p_k and p_{k+1} are the neighbourhoods. This optimisation function can be reformulated to be suitable for implementing dynamic programming with respect to an iterative cost function formulated as follows:

$$C(x,y) = \min_{j \in (-d_r, d_r)} C(x-1, y+j) + R_p(x,y) + \beta|j| - \frac{\gamma}{\sigma}\exp\left(-\frac{(y-r)^2}{2\sigma^2}\right) \quad (8)$$

$$\text{subject to } 2 \leq x \leq N, \quad 1 \leq y \leq M,$$

where β and γ are the weighting factors. The $C(x, y)$ is a 2D cost map. The global optimisation problem is the same to its sub-problem $C(x-1, y)$, $C(x-2, y)$, and *vice versa*. The radius r is a composition of the prediction calculated by the

local contrast method shown in the Appendix and the previous radius, i.e.

$$r_i = \frac{\hat{r} + r_{i-1}}{2}.$$

We set $C(1, y) = R_p(1, y)$ to be a boundary condition. If $d_r = 1$, the optimal index j^* can be determined by the following equation:

$$j^* = \arg\min_{j\in(-1,0,1)} C(x, y + j). \quad (9)$$

Therefore, the index can be stored in the coordinate matrix $X(x, y) = y + j^*$. In this construction, small cost values indicate higher likely boundary information. The position with the minimum cost value in the cost map $C(x, y)$ is searched. With a backward search from N to 1 in matrix X, the complete coordinates $(p_1 p_2 p_3 \ldots p_N)$ of the artery boundary can be determined, which is the optimal solution to this problem.

Summary of the algorithm:

Step 1: Input the 1st image.
Step 2: Use the centre (c_x, c_y) and the radius to define an ROI on the input image as R_s. Apply the directional gradient on R_s, output R_e (Cheng et al. 2011). Normalise R_e, $-1 \le R_e \le 1$. Calculate the local contrast of R_s. Predict the radius using the local contrast (Appendix).
Step 3: Transform R_e to polar coordinate, output R_p.
Step 4: Apply the dynamic programming with the circle model and embed the predicted radius and the local contrast (Appendix) to the cost function [Equation (8)]. Output the SFA boundary coordinates. Transform the coordinates from polar to Cartesian coordinates. Use the elliptic fitting to smooth the boundary.
Step 5: Calculate the centre (c_x, c_y) and the radius of the boundary.
Step 6: Check if there is next image. If yes, input next image and go to Step 2. If no, stop the algorithm.

2.5 *Accuracy analysis*

The proposed system is applied and the SFA cross-sectional lumen area of each image is calculated for the following comparison. The comparison is performed by calculating their relative unsigned errors as follows:

$$\varepsilon_i = \frac{|A_{\text{Manual}}(i) - A_{\text{Automated}}(i)|}{A_{\text{Manual}}(i)} \times 100\%, \quad (10)$$

where $A_{\text{automated}}(i)$ and $A_{\text{Manual}}(i)$ are the areas calculated by the automated and the manual drawing on the image number i, respectively. The averaged errors (on 50 images) and its standard deviations can be calculated.

3. Results

We first demonstrate the results of each step described in Sections 2.3 and 2.4. Then the results of accuracy and stability analysis are shown. Figure 3 shows the results described in Section 2.3. Figure 3(a) is the result after the top-hat transform on the sub-image extracted from the variance image. Figure 3(b) is its binarisation using the Otsu's method. Since it contains some noises, the following opening operation [Figure 3(c)] is applied to remove the unexpected noises and cut off possible connection between two vessels. All vessels are detected and their centres, long and short axes lengths, are calculated [Figure 3(d)]. Any vessel area which is smaller than a given threshold is deleted. This is to convince that all the smaller vessels will not be included so that the risk of missing identification can be decreased. Three features are calculated. The values from 1 to 3 [labelled in Figure 3(e)] are 2.13, 2.04 and 2.84, with the weighting factor $\alpha = 2$. Finally, the SFA is identified in Figure 3(f) which has the least cost value in Equation (6).

Figure 4 shows the results of the method described in Section 2.4. Figure 4(a) is the matrix R_p, which is the polar

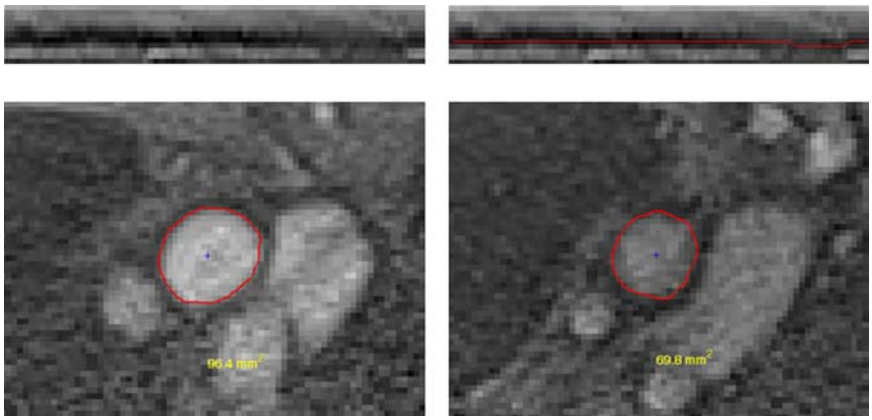

Figure 4. Results of Section 2.4. (a) The directional gradient R_p of the ROI sub-image R_e. (b) The curve found by the dynamic programming. (c) The detected curve is transformed from the polar coordinates to the Cartesian coordinates that represents the artery's boundary. (d) Another example that has less contrast on the boundary.

transform of R_e. Figure 4(b) is the resultant curve of dynamic programming superimposed on R_p. The curve is transformed from the polar coordinates to the Cartesian coordinates, which represents the boundary of the SFA [Figure 4(c)]. Figure 4(d) shows another example having a less local contrast.

Figure 5 shows the results of nine sequential images and their corresponding detected boundaries. They are organised in a 3×3 matrix. In each element of the matrix, the upper image is the raw sub-image and the lower image has its result superimposed on it. From the results, we can see that the first seven images in the artery's boundaries are vague. Even for a medical expert, it is very difficult to define their boundaries. Our algorithm can overcome this difficulty by using the local contrast as a guide to predict the area in these vague images. Therefore, the dynamic programming has the prior knowledge about the boundary location. All detected boundaries by the dynamic programming have been processed by an ellipse fitting (Fitzgibbon et al. 1999).

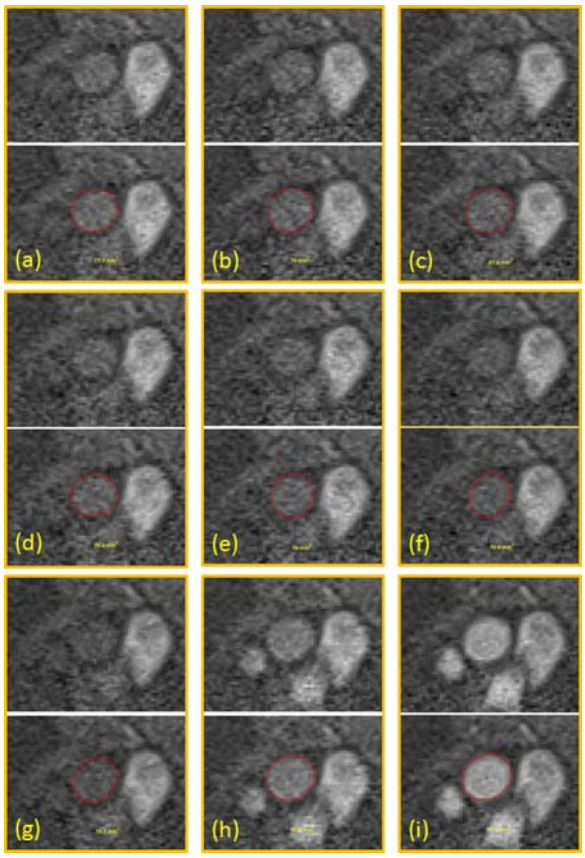

Figure 5. Results of Section 2.4. Nine sequential results are shown here. The boundaries are vague in the first seven images. They are hard to tell the exact boundaries. However, based on the help of the local contrast, we are able to predict the radii of the lumen of artery and guide the dynamic programming to detect the boundary.

Figure 6 shows the GUI of this system. The fully automated algorithm and manual tracing function are embedded together. The manual tracing function offers the sub-pixel possibilities in tracing the boundary for the experts.

Figures 7 and 8 provide the Bland–Altman plots of two sequences. The results of the automated detection of the cross-sectional area of each image in a sequence are compared to that of the manual tracings. Most of them are within two standard deviations. The average relative unsigned errors for sequences 1 and 2 are $2.6 \pm 2.8\%$ and $2.4 \pm 2.9\%$, respectively. The results demonstrate the system's ability to replace the expert's manual work.

Figure 9 illustrates the result of sequence 1. Notably, the system is able to detect the decrease in artery's area (around image number 6), which is a physiological phenomenon. This is the most difficult issue because the artery's boundary in this phase is unclear and it has the least image contrast. Sometimes even experts cannot tell exactly where the boundary is.

The computer system has Intel® Core™ 2 CPU T5600, 1.83 GHz, with 2 GB RAM. All programs are designed based on the Matlab platform (The MathWorks, Natick, MA, USA, 2008). The computation time for each image is around 0.5 s.

4. Discussions

To resolve the first issue described in Section 2.3, we used a local contrast to guide the boundary identification based on our observed fact that the contrast curve reveals the area-changing curve. The curve of the local contrast is very similar to the curve of artery's cross-sectional area. Especially it reveals the area dropped down around the image number 6, as shown in Figure 8.

In order to increase the accuracy, we used the standard image resize algorithm to increase the image and a scale factor of 2. Therefore, the dynamic programming can identify the boundary in the sub-pixel accuracy.

The proposed algorithm has two phases. The first phase is to localise and specify the centre of the SFA. The second phase is to identify the boundary of the SFA. It can be used to detect any boundary of arteries in MRI sequences with the prerequisite having the artery's centre position and its rough radius to define an ROI. Contribution of this study includes the proposed algorithm that not only can localise the centre of SFA but also can identify the boundary with a high accuracy even when the boundaries are vague in some images as shown in Figure 5.

Our MRA image sequences have been acquired using the gating technique: i.e. the ECG was used as a trigger to separate a heart cycle to 50 time gates. The danger of inconsistent solutions from frame to frame has been somehow alleviated by calculating the local contrast to predict the SFA cross-sectional area size and embed the

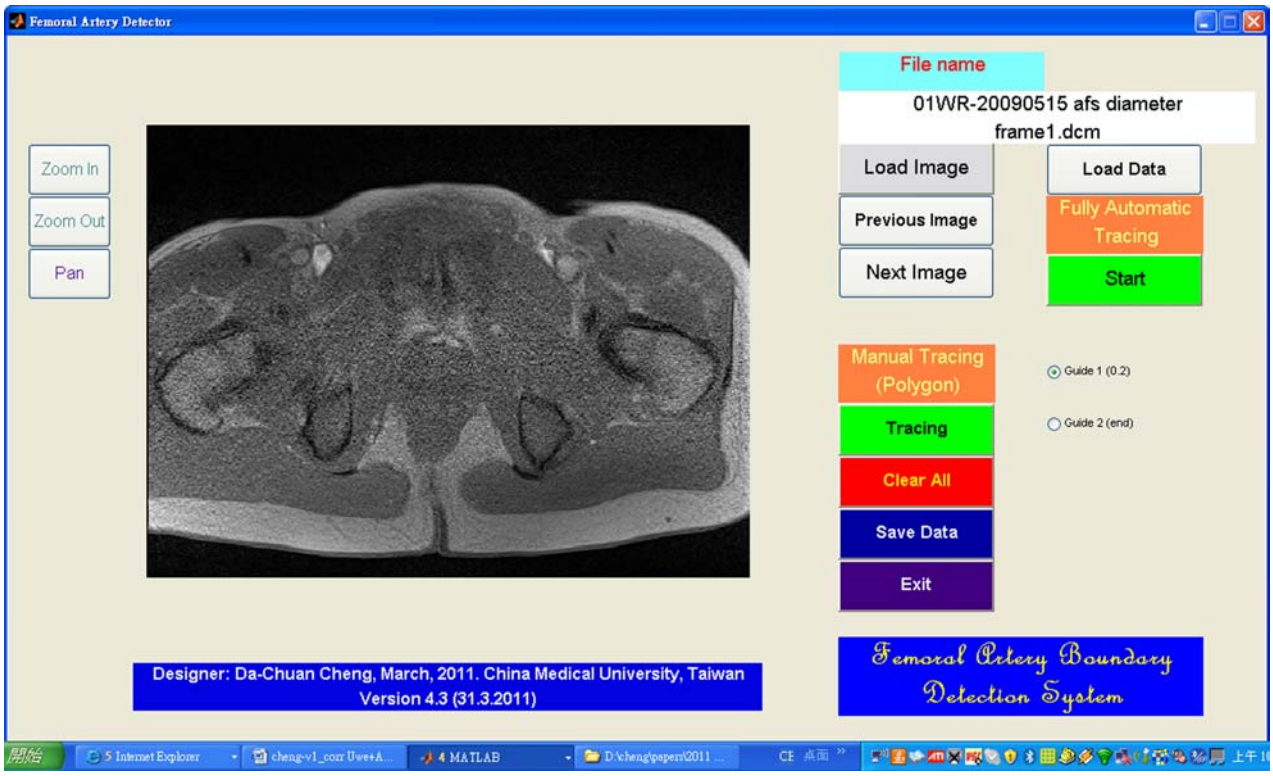

Figure 6. The GUI is developed to operate the system easily. It is based on the Matlab platform. The manual drawing function is also provided for the experts to trace the artery boundaries for comparison with the automated results.

predicted radius into the cost function used in the dynamic programming. However, we also observed that in an extreme situation when the human being cannot recognise the boundary, the radius prediction might also fail.

In comparison to the boundary detection of the carotid artery in MRI sequences (Cheng et al. 2011), the proposed algorithm of this study has the robustness against noises. This is because the SFA has lower contrasts to its background in some images when the blood flow velocity is slow. Under this situation, the boundary is vague and almost impossible to be defined and detected. Based on the observed data, we found that the local contrast can offer

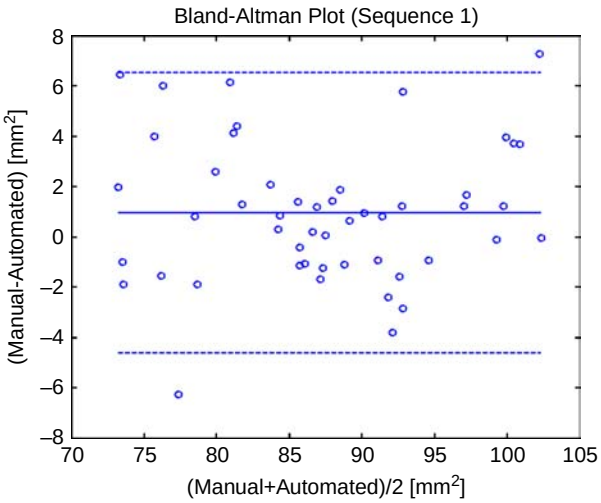

Figure 7. The Bland–Altman plot of sequence 1. The averaged relative unsigned error is 2.2 ± 2.8%.

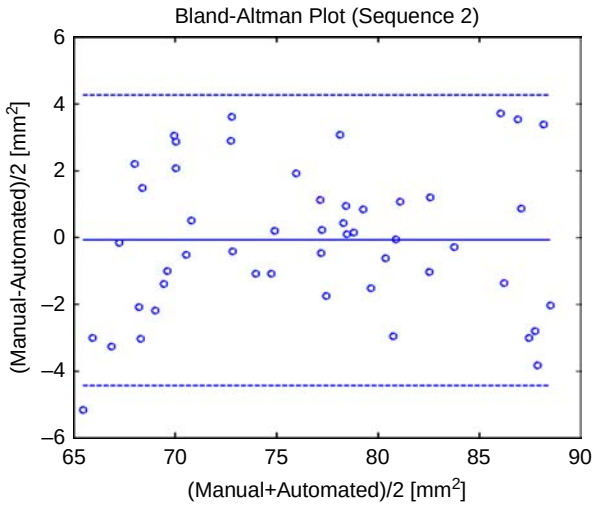

Figure 8. The Bland–Altman plot of sequence 2. The averaged relative unsigned error is 1.8 ± 2.2%.

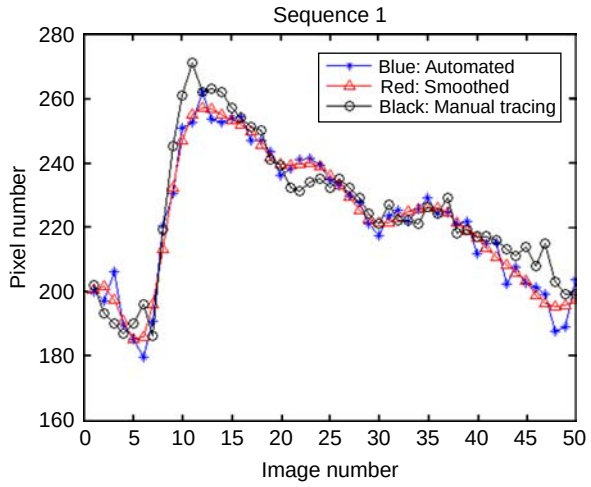

Figure 9. The cross-sectional area of artery changing with respect to time (sequence 1). The unit in the *y*-axis is pixel (pixel size = 0.3906 mm^2). The *x*-axis unit is the image number. The curves denoted by '∗', 'Δ' and 'o' are the automated result, smoothed automated result and the manual tracing gold standard.

important information to predict the area changes during the whole sequence. The mathematical model was developed in this study to show the correlation between the contrast and the cross-sectional area (see Appendix). In this study, we used the observed information to guide the dynamic programming to detect the boundary in a high accuracy.

The parameter β in Equation (8) controls the continuity of the boundary. If β is increased, then a smoother contour is obtained. Here β is fixed to be 1. The parameter γ is the weighting factor, which controls the strength effect of the radius prediction on the final contour resulted from the dynamic programming minimisation process. The value of γ is determined by an equation related to the local contrast as follows: $\gamma(i) = 1 + 0.5\sqrt{\text{contrast}(i)}$, where contrast($i$) denotes the normalised ith image local contrast calculated from R_s. If the local contrast is larger, it means that the boundary is visible so that the radius prediction is reliable. On the contrary, if the local contrast is smaller, it means that the boundary is vague and the radius prediction is not so reliable. However, the radius r used in Equation (8) is a composition of the prediction and the previous radius. Therefore, we still have a control on the radius so that the risk of inconsistent solution from frame to frame is limited.

A long acquisition time is necessary to ensure the high-resolution image quality. This is a precondition for the accurate vessel boundary detection. In the MRI acquisition process, the subjects were fixed with their lower extremities on a table. The compliance could be excellently seen throughout all examinations. Since all subjects refuse the injection of contrast media, the intraluminal signal intensity depends only on the inflow effect. This flow-dependent signal provides the critical factor for the border detection in the end-diastolic phase.

Moreover, the subjects in this study are healthy sporters. Therefore, there are no abnormal phenomena such as plaques attached on the SFA wall or lipid deposition. This is the reason we applied the elliptic model on the wall boundary in the last step of the second algorithm. However, this algorithm is available to deal with the abnormal cases. In such cases, the algorithm has to be minor modified. For example, the circle model and the elliptic model should be removed, since the artery wall is no more elliptic or round on the cross-sectional view in the MRA images.

5. Conclusion

We have developed a fully automated system that is able to detect the centre position of SFA and then identify its boundary. Regarding the accuracy, the average relative unsigned error is 3.1 ± 3.1% in five sequences compared to the manual tracings. The system proposed in this study is reliable with repeatable results that has the potential of replacing the expert's manual work.

Acknowledgements

This work was supported, in part, by the German Research Foundation ('Deutsche Forschungsgemeinschaft', DFG), under Grants SCHU 2514/1-1 and SCHU 2514/1-2 and by the National Science Council (NSC), Taiwan, under Grant NSC 100-2221-E-039-001.

Competing interests: The authors have no competing interests.

Authors' contributions: DCC and TCH have contributions on engineering aspects including: designed the software system of SFA wall detection, wrote the most part of the manuscript, and performed all experiments shown in this paper. AST and UHS have contributions on medical aspects including: designed the medical experiments, built the gold standard (manual drawings of SFA wall), and helped in manuscript writing. All authors have read and approved the final manuscript.

References

Cheng DC, Billich C, Liu SH, Brunner H, Qiu YC, Shen YL, Brambs HJ, Schmidt-Trucksäss A, Schuetz UHW. 2011. Automatic detection of the carotid artery boundary on cross-sectional MR image sequence using a circle model guided dynamic programming. Biomed Eng Online. 10(26):1–16.

Cheng DC, Jiang X. 2008. Detections of arterial wall in sonographic artery images using dual dynamic programming. IEEE Trans Inf Technol Biomed. 12(6):792–799.

Cheng DC, Schmidt-Trucksäss A, Liu CH, Liu SH. 2010. Automated detection of the arterial inner Walls of the common carotid artery based on dynamic B-mode signals. Sensors. 10(12):10601–10619.

Dasgupta S, Papadimitriou CH, Vazirani UV. 2008. Algorithms. McGraw-Hill.

Dinenno FA, Tanaka H, Monahan KD, Clevenger CM, Eskurza I, DeSouza CA, Seals DR. 2001. Regular endurance exercise

induces expansive arterial remodelling in the trained limbs of healthy men. J Physiol. 534(Pt 1):287–295.

Domínguez AR, Nandi AK. 2007. Improved dynamic programming based algorithms for segmentation of masses in mammograms. Med Phys. 34(11):4256–4269.

Dougherty ER. 1992. An introduction to morphological image processing. SPIE-International Society for Optical Engine: Bellingham, Washington, USA.

Doulaverakis C, Papadogiorgaki M, Mezaris V, Billis A, Parissi E, Kompatsiaris I. 2010. IVUS image processing and semantic analysis for cardiovascular diseases risk prediction. Int J Biomed Eng Technol. 3(3/4):349–374.

Fitzgibbon A, Pilu M, Fisher RB. 1999. Direct least square fitting of ellipse. IEEE Trans Pattern Anal Mach Intell. 21(5): 476–480.

Gorban AN, Zinoyyev AY. 2009. Principal graphs and manifolds. In: Olivas ES, editor. Handbook of research on machine learning applications and trends: algorithms, methods and techniques. Hershey: Information Science Reference, IGI, Global.

Huonker M, Schmidt A, Schmidt-Trucksäss A, Grathwohl D, Keul J. 2003. Size and blood flow of central and peripheral arteries in highly trained able-bodied and disabled athletes. J Appl Physiol. 95(2):685–691.

Jiang J, Haacke EM, Dong M. 2007. Dependence of vessel area accuracy and precision as a function of MR imaging parameters and boundary detection algorithm. J Magn Reson Imaging. 25:1226–1234.

Jolliffe IT. 1986. Principal component analysis. Springer-Verlag.

Kim D-Y, Park J-W. 2004. Computerized quantification of carotid artery stenosis using MRA axial images. Magn Reson Imaging. 22:353–359.

Langille B, O'Donnell E. 1986. Reductions in arterial diameter produced by chronic decreases in blood flow are endothelium-dependent. Science. 231:405–407.

Law MWK, Chung ACS. 2007. Weighted local-variance based edge detection and its application to vascular segmentation in magnetic resonance angiography. IEEE Trans Med Imaging. 26(9):1224–1241.

Liang Q, Wendelhag I, Wikstrand J, Gustavsson T. 2000. A multiscale dynamic programming procedure for boundary detection in ultrasonic artery images. IEEE Trans Med Imaging. 19:127–142.

Otsu N. 1979. A threshold selection method from gray-level histograms. IEEE Trans Sys Man Cybern. 9:62–66.

Radegran G, Saltin B. 2000. Human femoral artery diameter in relation to knee extensor muscle mass, peak blood flow, and oxygen uptake. Am J Physiol Heart Circ Physiol. 278:H162–H167.

Schmidt-Trucksäss A, Schmid A, Brunner C, Scherer N, Zäch G, Keul J, Huonker M. 2000. Arterial properties of the carotid and femoral artery in endurance-trained and paraplegic subjects. J Appl Physiol. 89:1956–1963.

Tang J, Acton ST. 2004. Vessel boundary tracking for intravital microscopy *via* multiscale gradient vector flow snakes. IEEE Trans Biomed Eng. 51(2):316–324.

Thijssen DHJ, De Groot PCE, Smits P, Hopman MTE. 2007. Vascular adaptations to 8-week cycling training in older men. Acta Physiol. 190:221–228.

Zhu H, Liang Y, Friedman MH. 2002. Year IVUS image segmentation based on contrast. Proc SPIE. 4684:1727–1733.

Appendix

The reason that the local contrast reveals the information of arterial cross-sectional area is described as follows. The local contrast is defined to be the total variance of the ROI extracted from the MRA image. We define three areas (Figure 10). The relationship between the total variance and the variances of the three areas can be formulated as follows:

$$\sigma^2 = \frac{1}{N}\sum_{i}^{N}(g_i - G)^2$$

$$= \frac{1}{N}\left[\sum_{g_i\in\Omega_1}(g_i - G)^2 + \sum_{g_i\in\Omega_2}(g_i - G)^2 + \sum_{g_i\in\Omega_3}(g_i - G)^2\right]. \tag{11}$$

Since the exact boundary locates in the sub-region Ω_2, using the right-hand side of equation cannot compute the cross-sectional area. Similarly, we assume the artery's radius to be r, where $r_1 < r < r_2$. To solve this problem, we use sampling to replace g_i in each sub-region. The formula can be rewritten as follows:

$$\sigma^2 = \frac{1}{N}\sum_{i}^{N}(g_i - G)^2$$

$$\cong \frac{1}{N}\left[\pi r^2(\hat{g}_1 - G)^2 + (N - \pi r^2)(\hat{g}_2 - G)^2 + \varepsilon'\right], \tag{12}$$

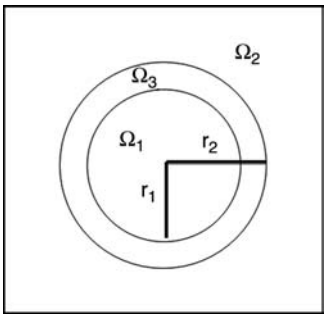

Figure 10. The model used to calculate the local contrast and predict the cross-sectional area of the SFA.

where the samplings $\hat{g}_1$ and $\hat{g}_2$ are the mean grey values of region Ω_1 and Ω_2, respectively; G is the mean grey value of the whole region and ϵ is the error. Therefore, the area can be estimated by

$$\pi r^2 \cong \frac{N(\sigma^2 - (\hat{g}_2 - G)^2)}{(\hat{g}_1 - G)^2 - (\hat{g}_2 - G)^2} + \varepsilon. \tag{13}$$

Through this formula the radius of the artery can be predicted before the boundary detection. This prediction is embedded into the cost function of the dynamic programming to guide the boundary identification as shown in Equation (8).